Journal of Building Engineering 87 (2024) 109051

Contents lists available at ScienceDirect

Journal of Building Engineering

journal homepage: www.elsevier.com/locate/jobe

Structural characterisation and reactivity measurement of chemically activated kaolinite

Adrian Alvarez-Coscojuela, Jofre Mañosa, Joan Formosa, Josep Maria Chimenos *

Departament de Ciència de Materials i Química Física, Universitat de Barcelona, Martí i Franquès 1, 08028, Barcelona, Spain

A B S T R A C T

This study examines the structural evaluation of differently activated kaolins for potential use as supplementary cementitious materials (SCM) or as precursor for alternative cementitious materials (ACM). Chemical activation involved amorphizing the kaolinite structure using varying phosphoric acid concentrations, reaction times, and temperatures. Metakaolin obtained via thermal activation served as a comparison. Inductively Coupled Plasma – Optical Emission Spectroscopy (ICP-OES) characterization of the activating solutions revealed phosphoric acid activation leading to dealumination in kaolinite structures, with temperature emerging as the most significant parameter. X-ray diffraction (XRD) confirmed amorphization, attributed to the dealumination process causing Al loss and creating new Si–O–Si interlayered bonds, as monitored by ^{29}Si magic-angle spinning nuclear magnetic resonance (MAS NMR) tracking the change from Q^3 to Q^4 environments. Furthermore, pozzolanic activity was assessed through $Ca(OH)_2$ consumption and reaction heat release via modified Chapelle and R^3 tests, respectively. Kaolinite subjected to intensive chemical activation exhibited high reactivity and increased specific surface area, indicating its potential as a pozzolanic material. *Keywords*: Kaolin; Chemical activation; Supplementary cementitious materials; Alternative cementitious materials; Dealumination; Pozzolanic reactivity.

1. Introduction

Cement production originates around 5–7% of carbon emissions worldwide [1]. Production of conventional clinker requires a large amount of energy during the sintering process, burning at 1450 °C raw materials thus causing an elevated carbon footprint [2]. The environmental impact of construction forces the contemporary industry to face the challenge of developing novel cement alternatives capable of minimizing carbon footprint. Partially replacing Portland cement (PC) with supplementary cementitious materials (SCMs), which do not involve any clinkering process, has emerged as a strategy for developing new sustainable types of cement [3,4]. The addition of SCMs is projected to decrease drastically the greenhouse gas emissions by reducing PC percentages using by-products from different sectors or elaborated materials with less energy demand [5]. Furthermore, alternative cementitious materials (ACMs) rise as a suitable option to reduce more significantly CO_2 emissions since ACMs do not incorporate PC in their composition [6]. SCMs and ACMs production cannot cover the huge demand for cement [7]. Hence, kaolin's importance is remarkable due to its widely available access and its potential application as a precursor for cement [8].

Clays are in major recognition since they performed as ceramics and construction materials in ancient ages, even before they were scientifically well-defined [9]. Clays and clay minerals are in great abundance in topsoils around the world, with silica and alumina constituting 75 wt% of the Earth's crust [10,11]. Their widespread availability promoted that the clay-research activities began an expansion in multiple scientific disciplines.

In structural terms, clays belong to phyllosilicates groups, characterized by their sequential polymeric sheets [12]. Clay morphology essentially consists of various combinations of two chemically different overlapping sheets (mostly 2:1 or 1:1 sequences). The first sheet is a 2-D layer formed by hexagons made up of SiO_4 tetrahedra units bonded simultaneously. The other sheet is comprised

* Corresponding author.
E-mail address: chimenos@ub.edu (J.M. Chimenos).

https://doi.org/10.1016/j.jobe.2024.109051
Received 10 November 2023; Received in revised form 8 March 2024; Accepted 12 March 2024
Available online 13 March 2024

of octahedral $AlO_4(OH)_2$ units, where Al is coordinated to six oxygen atoms, sharing four oxygen edges between octahedron units [12]. Both sheets are connected by the Si–O apical oxygen atoms, forming a crystalline structure bonded by covalent bonds, while the interlayer connections are formed by hydrogen bonds [13]. Kaolinite is a type of clay structured with a 1:1 lamellar disposition, which contributes to its remarkable stability. The well-packed disposition of kaolinite structures explains their poor reactivity performances [14].

Therefore, clay activation processes are designed to alter kaolinite's structural stability by inducing amorphization, thereby enhancing its reactivity and enabling improved reaction capabilities. Thermal and mechanical activations are the most studied activation mechanisms [15–17]. Structural disorder in kaolinite is commonly induced by thermal treatments. Submitting kaolin to temperatures between 600 and 750 °C leads to the dehydroxylation of kaolinite and its crystalline structure transformation into an amorphous phase named metakaolin, which possesses a high ability to react [15,18]. Recent progress on SCMs is based on metakaolin because clay calcination takes only 10% of the energy associated with clinker sintering procedures [19]. On the other hand, mechanical activation (MA) is based on causing the loss of crystallinity of kaolinite structure by grinding with milling equipment [16,17,20,21]. Milled structures are usually obtained in chemical-free and low-energy requirement processes, so MA is well-known as a sustainable activation treatment [22].

Alternatively, chemical activation (CA) of clays can be achieved using both phosphoric mineral acids and alkaline media [23]. These attacks result in a cement with an amorphous structure and good mechanical properties known as geopolymer [24,25]. The idea of this study is to create a precursor as SCM to replace PC rather than cement itself. So, a novel method of clay activation will be tested to amorphise kaolin and thus impart a certain degree of reactivity to the final material. Currently, there are no studies describing chemical activation of clay as a cement precursor in the literature, so this study offers a different activation route to the common kaolin activations. For these chemical activations, optimal parameters were established to induce high amorphization levels in clay structure which were carried out by acidic chemical attacks with different combinations of temperatures, phosphoric acid concentrations and reaction times. A special emphasis was put on the usage of phosphoric acid since it is used as a reagent for acid-based geopolymers [26].

This work aims to synthesise a new clay-based SCM or ACM precursor with high reactivity levels, thus emerging a novel effective method to replace PC. For this purpose, this work is divided into two distinct parts; the first part focuses on the structural characterisation to evaluate the chemical changes within the kaolinite structure during the CAs as well as following its amorphization evolution. The second part focuses on the reactivity of the final material by testing its pozzolanic activity using two different methods to quantify its effectiveness as an SCM or ACM precursor.

2. Materials and methods

2.1. Materials

The raw kaolinitic clay (K) used during the chemical activation (CA) without any further purification was proportionated by the Spanish company Minerals i Derivats, S.A. The chemical composition of the raw clay was analyzed by X-ray fluorescence (Table 1) with a Panalytical Philips *PW* 2400 sequential X-ray spectrophotometer equipped with UniQuant® V5.0 software. The crystalline composition was detected with X-ray diffraction (XRD) using a Bragg-Brentano PANalytical X'Pert PRO MPD alpha1 powder diffractometer with CuKα1 radiation ($\lambda = 1.5406$ Å). The measuring time was 100 s and five scans were performed for each sample. The experimental configuration was: a focalizing Ge (111) primary monochromator, step size of 0.026°, anti-scatter slit of 4° and Soller slit of 0.04 rad. The principal crystalline phases of the starting clay material were determined by using X'Pert HighScore software.

For the CA, a commercial phosphoric acid with an 85 wt% content of H_3PO_4 was provided by Labkem, which was then diluted with distilled water until achieving the required molar concentrations. For both pozzolanic activity tests the purchased reagents were: calcium oxide and potassium sulphate from Thermoscientific and, potassium hydroxide from Fisher Scientific®. Furthermore, Labkem also provided the hydrochloric acid 0,1 N and D(+)–Sucrose AGR required for the titrations.

2.2. Chemical and thermal activation methodology

A schematic diagram of the chemical activation procedure on experimental and characterisation terms is implemented in Fig. 1. Chemical activation was carried out with an H_3PO_4 solution in contact with the raw kaolinite material in a spherical flask of 250 mL equipped with a reflux system to condense water at the corresponding working temperatures. Taking into consideration preliminary CA trials, the solid-solution ratio was fixed to 1/10 to ensure high kaolin-phosphoric acid interactions without forming a cementitious paste and avoiding another parameter to no further experimental complexity. After vigorously mixing, to stop the reaction taking place, the solid was filtrated and then, severely washed with distilled water (approximately 500 mL) to remove H_3PO_4 from the unreacted remaining particles. Before analysis, the obtained solid was dried overnight in an oven at 105 °C. Simultaneously, the activating phosphoric solution was filtered and subsequently stored in a refrigerator at a temperature of 15 °C.

Different parameters were studied to optimize the chemical acidic activations of kaolinite clay. The effect of three parameters on CA

Table 1
XRF analysis of the raw kaolin material.

Compounds	SiO_2	Al_2O_3	K_2O	Fe_2O_3	CaO	TiO_2	Na_2O	MgO	P_2O_5	MnO	LOI[a]
wt. %	49.85	36.31	0.69	00.47	0.16	0.15	0.13	0.11	0.08	0.00	12.03

[a] LOI: Loss on ignition at 1100 °C.

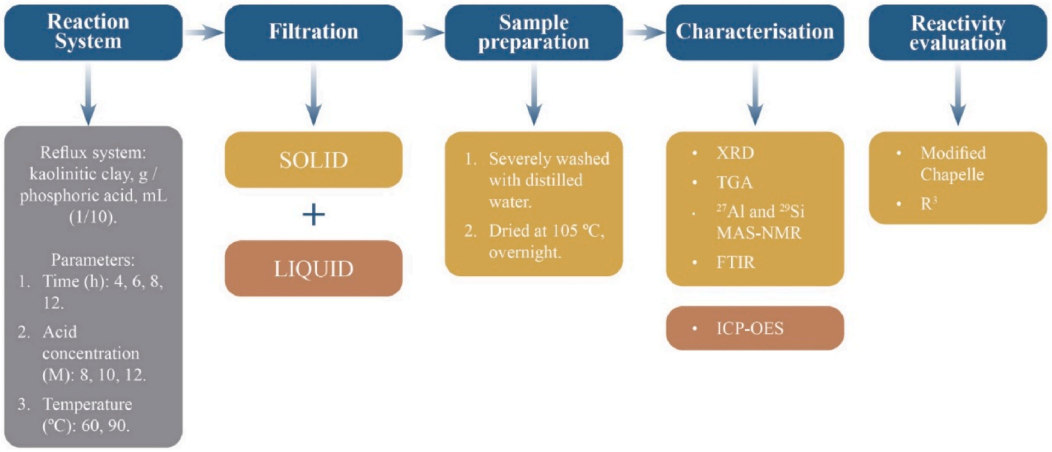

Fig. 1. Experimental procedure scheme of chemical activation.

was studied, namely (i) reaction time (4 h, 6 h, 8 h, and 12 h), (ii) temperature (60 °C and 90 °C), and (iii) phosphoric acid concentration (8 M, 10 M and 12 M). For every chemically activated kaolinite, a corresponding notation is employed following the nomenclature *KP_t_[H_3PO_4]_T*, wherein *KP* refers to K activated with phosphoric acid, *t* denotes the reaction time, *[H_3PO_4]* indicates the phosphoric acid concentration and *T* is the working temperature. Consequently, the experimental design comprised 24 different combinations.

Based on ICP-OES results, five different samples from five different CAs were selected as representative samples (Table 2) in the Results and Discussion section. KP_12_12_90 performs as the most aggressive CA, followed by KP_12_10_90 and KP_12_8_90, which represent moderately intensive CA and will be used for evaluating the concentration contributions to CA. Meanwhile, KP_12_12_60 acts as a comparative sample to estimate the temperature effect. KP_4_8_60 sample, referring to the less intensive treatment, will be used to study the slight differences achieved in the resultant materials compared to the raw kaolin.

Moreover, the raw kaolin was also thermally activated (750 °C for 6 h) to obtain metakaolin (MK), so all characterised samples were compared with MK. In addition, MK is also useful to analyse and compare the synthetic precursors' efficiency through pozzolanic activity tests, which are described below. The raw K was also structurally defined as well as its reactivity was tested. Both K and MK were assessed for comparison purposes.

2.3. Characterisation

2.3.1. Inductively Coupled Plasma – Optical Emission Spectroscopy (ICP-OES)

ICP-OES was first performed to evaluate the content of different dissolved species resulting from the treated kaolinite. The chemical activation was performed with different parameters. So, ICP-OES tracked all conditions: reaction time, temperature, and phosphoric acid concentration to evaluate the chemical activation efficiency.

2.3.2. X-ray Diffraction (XRD)

To follow the structural distortion promoted by the chemical activation procedures, the XRD patterns were analyzed, utilizing the same conditions described in Section 2.1, focusing on the kaolinite reflections.

2.3.3. Thermogravimetric analysis (TGA)

The effect of CA on the hydroxyls of the kaolinite structure was evaluated through thermogravimetric analyses using an SDT 600 (TA Instruments) from 30 to 1000 °C, with a heating rate of 10 °C·min^{-1} and a synthetic air flux of 50 mL min^{-1}.

2.3.4. ^{27}Al and ^{29}Si MAS NMR (magic angle spinning nuclear magnetic resonance)

To define the near-neighbouring of Al and Si atoms the ^{27}Al and ^{29}Si MAS NMR spectra were recorded at room temperature in an

Table 2
Samples under study.

Samples	Activation methodology	Reaction time (h)	Phosphoric acid concentration (M)	Temperature (–C)
MK	Thermal	6	–	750
KP_12_12_90	Chemical	12	12	90
KP_12_10_90	Chemical	12	10	90
KP_12_8_90	Chemical	12	8	90
KP_12_12_60	Chemical	12	12	60
KP_4_8_60	Chemical	4	8	60
K	–	–	–	–

AVANCEIII HD 600 (Bruker AXS) spectrometer using a double resonance CPMAS probe of 4.0 mm at a spinning rate of 14 kHz and 13 kHz, respectively. The magnetic field was 14.1 T corresponding to a ^{27}Al resonance frequency of 156.37 MHz and ^{29}Si resonance frequency of 119.22 MHz. ^{27}Al MAS NMR spectra were recorded with an excitation pulse of 0.7 μs and 1-s delay with ^{1}H decoupling (^{27}Al Hpdec with cw decoupling sequence for Al) and summing up 2000 scans, while ^{29}Si MAS NMR spectra were recorded with an 8.5-μs 90° pulse and 60-s delay with ^{1}H decoupling (^{29}Si Hpdec with cw decoupling sequence for Si) and summing up 1000 scans. The ^{27}Al chemical shifts are referenced to $Al(NO_3)_3$, whereas the ^{29}Si chemical shifts are referenced to trimethylsilyl group, $(CH_3)_3Si$-.

2.3.5. Fourier-transform infrared spectroscopy (FTIR)

In addition, to support the structural evolution, the A Spectrum Two™ PerkinElmer spectrometer in attenuated total reflectance (ATR) mode was employed. The spectral evolution of the samples was evaluated through different chemical activations with 32 scans over the range of 4000–450 cm^{-1} at a resolution of 4 cm^{-1}. The spectra were enclosed to the interest regions where Si–O, Al–O, and OH- bonds are commonly scanned.

2.4. Pozzolanic activity tests

2.4.1. Modified Chapelle test

The modified Chapelle test was carried out by measuring the $Ca(OH)_2$ consumption when it is combined with aluminosilicate species in an isolated environment [27]. This test aims to quantify the capability of the aluminosilicate sources to react with Ca units, [28–30]. 1 g of pozzolanic material and 2 g of powdered CaO were added to 250 mL of distilled water. The mixture was then vigorously stirred for 16 h at 90 °C and was controlled by refrigerant equipment. A control experiment (blank test) without the pozzolanic material was made under the same conditions. Once the reaction system cools down for 1 h, the solution is added to 250 mL of sucrose 0.7 M and mixed for 15 min. Then, approximately 150 mL of the pozzolanic system-sucrose resultant solution was filtrated and 25 mL were titrated with 0.1 N HCl and 4–5 phenolphthalein drops. To measure the portlandite ($Ca(OH)_2$) fixed by the SCM the following formula was used:

$$PA = 2 \cdot \frac{v1 - v2}{v1} \cdot \frac{74}{56} \cdot 1000 \quad \text{(Eq1)}$$

where PA (pozzolanic activity) refers to mg fixed $Ca(OH)_2$ g^{-1} of SCM; $v1$ is the required volume for titrating 25 mL of control solution (blank test); $v2$ is the required volume for titrating 25 mL of the solution where the pozzolanic reaction takes place. Two replicates were titrated three times to ensure repeatability.

2.4.2. R^3 test

To increase the accuracy of pozzolanic activity measurements in addition to corroborating the Chapelle test reliability, another route to test the reactivity was implemented. The R^3 test is based on measuring the heat released during the cement hydration reaction. This test provides a more accurate simulation of cement reactions compared to the modified Chapelle test. The main advantages that R^3 presents are the easy experimental procedure (rapid), the information obtained on clays reactivity (relevant) and its correlation with compressive strengths results (reliable) [31]. The pozzolanic reaction carried out involved the amorphous aluminosilicate phases and calcium hydroxide reagents, producing C–S–H and alumina phases [32].

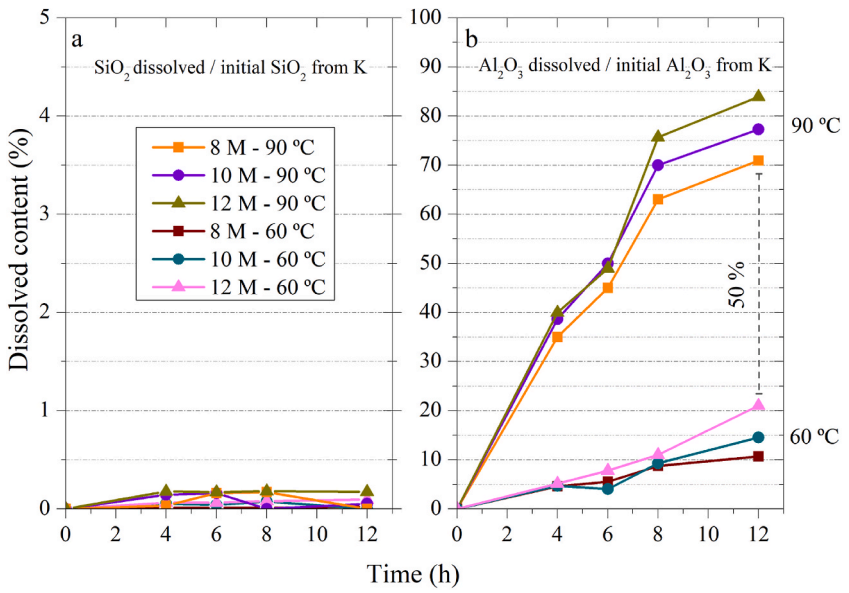

Fig. 2. Dissolved (a) SiO_2 and (b) Al_2O_3 from the treated clay dissolution at 60 and 90 °C determined by ICP-OES.

The mix of R^3 design was carried out following ASTM C1897 − 20 [33]. The chemically activated samples described in Table 2 were mixed with $Ca(OH)_2$ (1:3 ratio) and $CaCO_3$ (2:1 ratio) and mixed with a K_2SO_4 and KOH solution to obtain a paste (solution/solid ratio = 1.2). The solution was prepared by dissolving 4 g of K_2SO_4 and 20 g of KOH in 1 L of distilled water. The paste was obtained by mixing for 2 min at 880 rpm the solid mixture and the solution using a high shear mixer, and 15 g of paste was poured into a plastic ampoule. The heat of the reaction was measured for 6 days using an isothermal calorimeter TAM Air (TA Instruments). The calorimeter was set at 40 °C and a plastic ampoule with 9.4 g of water was used as a reference to avoid external temperature deviation. KOH and sulphates were added for an accurate reproduction of cement development and similar products' obtention. Nonetheless, some authors have remarked that K_2SO_4 presence can change the nature of the resultant phases, hence their side reactions must be considered in the calorimetry results for the $Ca(OH)_2$ consumption [34,35]. Moreover, the isothermal calorimetry starting data was recorded at 75 min to avoid unstable signals so the calorimeter could establish at 40 °C accurately.

2.4.3. Specific surface area

In addition, the Brunauer–Emmett–Teller (BET) method was also implemented to evaluate the specific surface area to compare the structural change in reactivity terms between samples. It was carried out with a Micromeritics Tristar 3000 device.

3. Results and discussion

3.1. Structural characterisation

3.1.1. ICP-OES

Quartz and silica do not present a clear mechanism of dissolution, nonetheless, Si–O bonds breakage is unlikely in acidic conditions [36]. As depicted in Fig. 2a, no substantial change in Si dissolution is achieved even with treatments at high temperatures, high H_3PO_4 concentrations, and the largest reaction time proposed. Only around 0.25% of the total SiO_2 available in kaolin is dissolved. This phenomenon could be attributed to silicon's chemical nature. SiO_2 consists of uncharged and strongly covalent bonded tetrahedrons containing Si^{4+} ions, which are non-metallic cation with low polarizability, thereby classifying it as an acid oxide [37]. ICP-OES of Si indicates that CA with phosphoric acid does not lead to the Si^{4+} units release from the kaolin structure.

On the other hand, Al dissolution has been achieved at different temperatures [38]. Commonly, acidic treatments on clay lead to the dealumination of aluminosilicate units [39,40]. As shown in Fig. 2b–a significant difference in the amount of dissolved Al under both working temperatures is observed. The dissolution of Al increases by approximately 50% at 90 °C compared to 60 °C after 12 h of reaction, leading to the formation of two distinct regions in the graph. Moreover, no plateau is reached which indicates that more quantity of aluminium could be available to be dissolved with longer treatments. At 60 °C there is a slight increase of the Al dissolved percentage comparing 8 M, 10 M and 12 M, especially for 8 and 12 h. A similar trend is observed in the case at 90 °C, wherein the difference in dissolved aluminium content can range from 11% to 13%, depending on the molarity of the H_3PO_4 solution used in the CA. The reaction time of K–H_3PO_4 systems exhibits more significant changes for Al dissolved content in the case of samples exposed to 90 °C, suggesting a lower reaction degree in 60 °C samples [41]. In conclusion, temperature emerges as the most critical parameter influencing the dissolution of Al, which incites kaolinite to be further amorphised.

The Al_2O_3 dissolved ratio directly depended on the CA treatment conditions. This particular fact can cause a significant mass loss of the required kaolin. In this sense, the loss of a high percentage of alumina should cause a major problem in the precursor obtention since a large amount of raw kaolin would be required for a very poor production yield.

3.1.2. XRD

Fig. 3 plots the crystallographic evolution of the mineral phases contained in K depending on the different CA indices implemented during the experimental procedure. The study was focused on the kaolinitic clay conversion degree into an amorphous material. The diffractograms presented in Fig. 3 correspond to the CA of 12 h of reaction time, as they were considered to show more significant changes. Most of the reflections are indexed to kaolinite and quartz. The presence of K-feldspar is observed for every sample also at

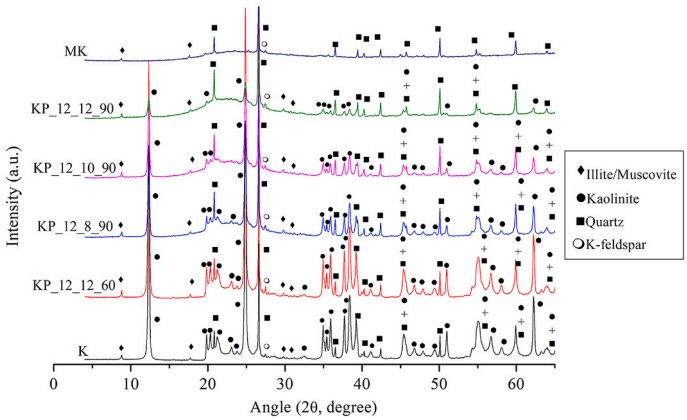

Fig. 3. XRD diffractograms of K, MK and chemically activated samples treated for 12 h.

27.5°(2θ). In addition to those main mineral phases, slight reflections in 8.8°, 17.7° and 29.9°(2θ) indicate the presence of minor species corresponding to illite and/or muscovite, which differentiation is very difficult due to their similar reflections. This is caused because their analogous structure can be only distinguished by their little chemical composition differences [42]. In addition, to follow the structural amorphization in acid-activated samples, the MK diffractogram was added. MK reflection peaks were attributed to unaltered quartz and muscovite/illite phase.

A visible difference in the diffractograms in the angle range between 20 ° and 30°(2θ) and 35 °–70°(2θ) of KP_12_12_90 (green line) and KP_12_12_60 (red line) is detected for kaolinite. Characteristic kaolinite reflections are significantly more reduced at 90 °C compared to CA at 60 °C, indicating that the dealumination alters and modifies kaolinite structures at higher temperatures. Increasing the phosphoric acid content from 8 M to 12 M intensifies the dealumination process of kaolinite, resulting in a significant decrease in its main reflections, which underscores the critical role of temperature and concentration in controlling the CA procedures [43]. Nonetheless, even the most intensive-activated samples still show kaolinite reflections with lower integral intensities (areas), suggesting that the kaolinite consumption is incomplete. Quartz is also detected for all samples after acidic activation, showing the already known great chemical stability without considerable changes between both work temperatures or different acidic concentrations [44].

Usually, the formation of newly amorphised phases can be described in XRD as a broad irregular hump-shaped peak around 20 °–30°(2θ) [13,45]. This typical broad peak is observed (seen in Fig. 4) from 15° to 33°(2θ) in samples with high temperatures and long reaction times for all phosphoric acid concentrations, demonstrating the formation of an amorphous phase and achieving a potential high-reactive clay precursor. The MK diffractogram presents a similar band in the same region. The diffractogram modifications according to the area of the amorphous irregular peak demonstrate that the degree of the amorphosity increases as the hump area becomes more extended and intense. So, the growth of the reflection curve is associated with a decrease in kaolinite content. It is also remarkable that no other crystalline phases are formed even with kaolinite consumption and a considerable amorphization degree is achieved.

In addition, in 1:1 typical kaolinite layer aluminium octahedra are exposed, so acid-base reactions can easily occur. Conversely, in the 2:1 layer, as aluminium species are found between two crystalline Si layers in a sandwich structure, the CA becomes further difficult. As a result, the area of illite/muscovite peaks does not exhibit a significant decrease while CAs are incremented (Fig. 4). K-feldspar remains also unaffected.

3.1.3. TGA

The dealumination process and crystalline kaolinitic content reduction induced by CA are also corroborated by thermogravimetric analysis. Fig. 5 reveals two steps of mass loss on K and treated samples. The first step involves the mass loss of physically absorbed water of kaolinite which occurs in the 0–200 °C range [46]. This step in the raw kaolin was found with a mass loss below 1 wt%. The observed mass loss value of about 2–2.4 wt% for treated samples corresponds to the interlayer and adsorbed water removal from the new structure. This provides more space for the physical arrangement of water due to the released aluminium than the initial kaolin. The second step produces around 13 wt% for the raw kaolin which is attributed to the dehydroxylation process of the kaolinite. This process reflects the structural modification during the heating of kaolinitic materials where the hydroxyl groups bonded to Al units are thermally removed as water, as reported in Eq. 2 [47,48]. This phenomenon occurs in the range of 400–700 °C accompanied by a 14 wt % approximately, a value that depends on particle size, impurities content, and heating rate, among others [49].

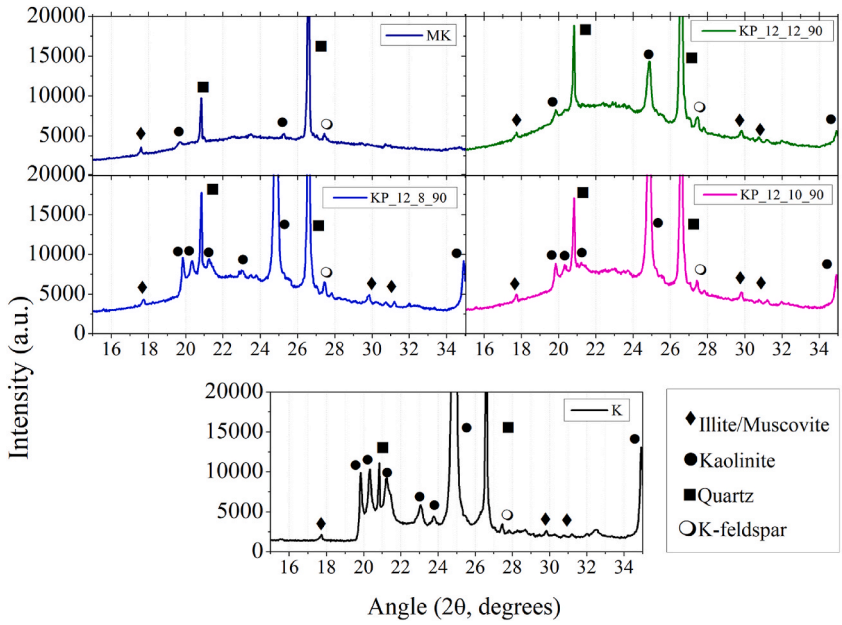

Fig. 4. XRD of K, MK, KP_12_12_90, KP_12_10_90 and KP_12_8_90 at 15 °–35° 2θ region.

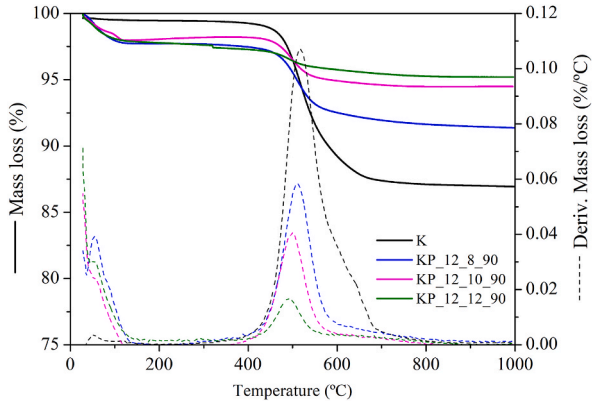

Fig. 5. TGA measurements of K, KP_12_8_90, KP_12_10_90, and KP_12_12_90 (solid line for mass loss, and dashed line for derivate of mass loss).

$$Si_2Al_2O_5(OH)_{4\ (s)} \rightarrow Al_2O_3{\cdot}2SiO_{2\ (s)} + 2H_2O_{\ (g)} \quad \text{(Eq.2.)}$$

In the TGA of chemically treated kaolins, mass loss is observed to occur in smaller percentages. So, the inner and surface Al–OH bonds are significantly decreased. This correlates with the ICP-OES results, confirming that the kaolinite's CA mechanism is based on its structure's dealumination. Consequently, TGA exhibits a consistent trend for all samples according to different dealumination degrees. As the Al–OH bonds decrease, a smaller quantity of mass is lost in the dehydroxylation process. This is due to H_3PO_4 first reacting with the Al–OH kaolinitic bonds, producing $AlPO_4$ species solved in the reaction medium [50,51]. KP_12_12_90, with 83.9% of Al_2O_3 solved (see Fig. 2) registers a mass reduction of only 2 wt%, while KP_12_10_90 and KP_12_8_90 presents a 3 wt% and 5 wt% of mass loss with an Al_2O_3 loss of about 77.3% and 70.9%, respectively.

In terms of the thermogravimetric studies related to amorphised kaolinitic clays, the dehydroxylation processes are normally found with a gradual mass loss through a wide range of temperatures, where the OH within the kaolinitic structure are removed according to

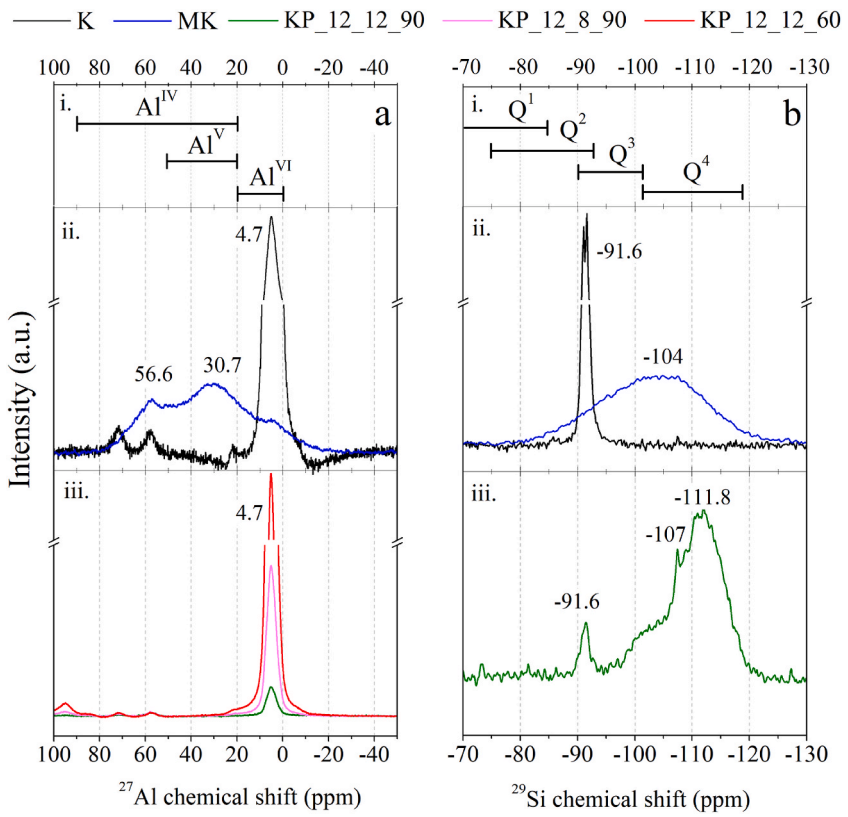

Fig. 6. Chemical changes of (a) Al and (b) Si near-neighbour surroundings of MK, KP_12_12_90, KP_12_8_90 and KP_12_12_60, and K surroundings.

the attaching degree to the structure depending on the amorphization levels [13]. In this study, the TGA mass loss jumps are established in a very slight temperature range. This indicates that all remaining Al–OH bonds in samples after acidic treatments offer the same structure, confirming that the remaining Al is found as crystalline kaolinite. This fact is further supported by the presence of kaolinite in each treated sample in the XRD study.

Furthermore, TGA supports that the newly vacant Si sites, formed during the removal of aluminium, are not finally reconverted into Si-OH species, as evidenced by the absence of any additional mass loss in the TGA. Hence, the restructuration of the resultant amorphous kaolinites of this work may proceed with new randomly distributed Si–O–Si interlayer bonds, ascribing the amorphization to Si layers only.

3.1.4. MAS NMR

^{27}Al MAS NMR reveals the Al surrounding environments of K and MK (presented in Fig. 6a–ii), and KP_12_12_60, KP_12_8_90, and KP_12_12_90, which are presented in Fig. 6a–iii. In the K spectrum, the appearance of a very intense and sharp peak at 4.7 ppm confirms the presence of the kaolinite structure overall kaolin, which corresponds to the hexa-coordinated Al [52]. There are other very small contributions attributed to K-feldspars (around 60 ppm) and illite (around 70 ppm) [22]. The MK spectrum shows three different resonances at 4.7 ppm, 30.7 ppm and 56.6 ppm, associated with Al^{VI}, Al^{V} and Al^{IV}, respectively [42,53–55]. Those species coexist in MK structures according to Loewenstein restrictions [56], which dictates that 5 or 4-coordinated Al cannot be straight bonded via one oxygen between them [57]. This means that Al^{VI} must be present even in amorphous clays as well as the impossibility to convert all Al^{VI} into lower coordination number species. Obtaining Al^{IV} and Al^{V} structures is of great importance since they can highly amorphise the kaolinite structure [58]. However, only the 4.7 ppm resonance is observed in the chemically treated samples as shown in Fig. 6a–iii, which is assigned to the remaining non-dealuminated regions of the kaolinite. According to the dealumination processes, the resonance intensities decrease while the CA became more aggressive, but no transition to less coordinated aluminium was achieved. This supports that the CA with phosphoric acid dissolves octahedral Al units entirely, so there are no partial reactions with the hydroxyl groups. As a result, there is no Al^{VI} transformation into Al^{V} or Al^{IV} species. This is in contrast with thermal and mechanical kaolin activations [22], raising an amorphization model without amorphised aluminium content. The illite peak is maintained during the CAs, confirming the previous hypothesis about the phosphoric acid's incapability to penetrate and react with aluminium in the 2:1 phyllosilicate layer. The resonation of K-Feldspar remained also.

^{29}Si MAS NMR was performed on K, MK and KP_12_12_90. The main resonance at −91.6 in the K spectrum is associated with the typical Si kaolinite surroundings with Q^3 environments (Fig. 6b–ii) [52]. In the transition traced by K to MK, the main spectrum intensity is transformed into a broadened and less intensive peak covering the region from −90 ppm to −120 ppm with a maximum of around −104 ppm. This confirms the rearrangement of Al_2O_3 and SiO_2 bonds during the clay dehydroxylation which leads to Q^3 and Q^4 environments. The sharp kaolinite band is still present in the KP_12_12_90 spectrum at lower intensities (Fig. 6b–iii), which indicates a partial distortion in the aluminosilicate layers explained by the remaining Q^3 contributions. Moreover, the transition from a sharp peak at −91.6 ppm to a broad peak with a maximum at around −111.8 ppm indicates the amorphization of the KP_12_12_90 structure [54,59]. The Si layers are severely affected by the dealumination promoted by CA since its typical Q^3 band experimented a

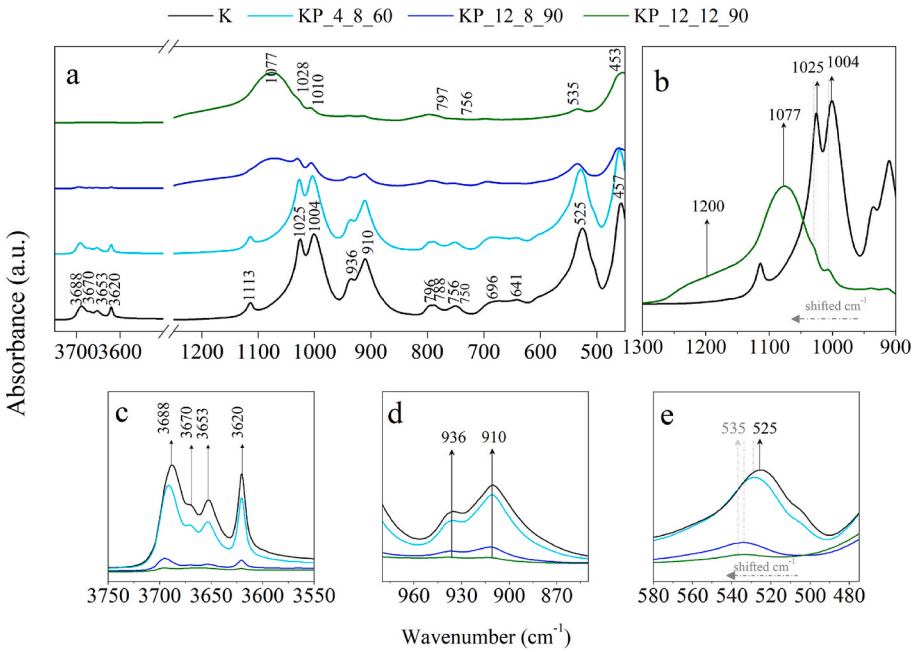

Fig. 7. K, KP_4_8_60, KP_12_8_90 and KP_12_12_90 FTIR spectra (a) at the regions between (b) 1300-900 cm^{-1} (c) 3750-3550 cm^{-1} (d) 980-850 cm^{-1} and (e) 580-475 cm^{-1}.

transition from Q^3 to Q^4 Si environments [12]. Moreover, the peak projected beyond the −111.8 ppm band at −107 ppm corresponds to quartz contribution [60]. The ^{29}Si NMR results are in accordance with XRD diffractograms which show an amorphised material with remaining traces of kaolinite and quartz. Accordingly, the amorphization of the resultant chemically activated samples is not induced by kaolinite Si–O–Si and Si–O–Al bonds rearrangement as the other activation procedures [22,61]. This fact can be observed in the comparison of MK and KP_12_12_90 spectra, which shows just one irregular broad peak unifying Q^3 and Q^4 contributions and two distinct contributions separated by Q^3 and Q^4 regions, respectively. So, it can be concluded that new randomly interlayered Si–O–Si (Q^4) bonds are formed once the Al is released.

3.1.5. FTIR

To complete the structural study, an FTIR analysis was also implemented (Fig. 7). The analysis is focused on the typical kaolinite regions: 3750-3550 cm^{-1}, 1300-900 cm^{-1}, 980-850 cm^{-1} and 580-475 cm^{-1}. The main bands of the kaolinite infrared spectrum are assigned according to bibliography research as follows: 3688 cm^{-1} corresponds to in-phase symmetric stretching of inner-surface OH groups. 3670 and 3653 cm^{-1} are related to stretching vibrations of inner-surface OH groups. 3620 cm^{-1} stretching is correlated with inner hydroxyl groups vibrations. 1113, 1025 and 1004 cm^{-1} are assigned to o the apical vibrations of apical Si–O bonds, in-plane Si–O–Si stretching vibrations, Si–O–Al vibrations, respectively. 936 and 910 cm^{-1} are related to inner surface hydroxyl groups Al–O–H vibrations and inner O–H vibrations in Al–O–H. 641 cm^{-1} is related to Si–O–Si bending, 525 cm^{-1} is attributed to Si–O–Al stretching, and 457 cm^{-1} is assigned to Si–O–Si bending [22,62,63].

Fig. 7a compiles the significant variation of the initial kaolin through different phosphoric acid treatments by substantial reductions of the characteristic kaolinite peaks. CA induced a new amorphous phase as is qualitatively detected by XRD and NMR studies. The KP_4_8_60 spectrum does not show an appreciable change in comparison with the raw kaolin spectrum because the distortion structure achieved is almost negligible. KP_12_8_90 spectrum shows the kaolinite peaks highly diminished while the KP_12_12_90 spectrum indicates the almost destruction of kaolinite since its corresponding peaks almost disappeared. The temperature performs as a more determinant experimental parameter than acid phosphoric concentration. Moreover, for the 12 h of time reaction and 90 °C treated samples, a new peak appeared at 1077 cm^{-1}, which was assigned to quartz presence [62,64]. Once chemical activation becomes more intense, kaolinite areas disappear due to the dealumination process. Consequently, the unmasking of the quartz peaks starts. For example, the 453 cm^{-1} band is slightly diminished compared to other kaolinite peaks due to the around 450 cm^{-1} Si–O vibrations of kaolinite and quartz coexistence [65]. Nonetheless, the only observable change in the spectrum is the disappearance of kaolinite content and the formation of a broader peak in the Si–O spectra region. Fig. 7b suggested the possibility of the existence of some amorphous silicates in 1090 cm^{-1} due to the broad band at 1077 cm^{-1} could hide them, in addition to the quartz contribution [64]. The wide shoulder around 1200 cm^{-1} is attributed to a combination of the poorly ordered kaolin within the same aluminosilicate structure [66].

In Fig. 7c, the region of the OH which comprised the kaolinite structure is observed [13]. That region gives fundamental information about the final structure of the clay since OH groups are responsible for the hydrogen bonds that connect the sequential kaolinite sheets between them, as well as covering the structural function with the Al octahedra units [67,68]. The consumption of OH bonds increases while the applied CAs are augmented, so the four peaks in the 3750 - 3550 cm^{-1} region decrease. This is due to the acid-base reaction between the H_3PO_4 and hydroxyl groups. This can also be observed in Fig. 7d, where both 936 cm^{-1} and 910 cm^{-1} Al–OH vibrations undergo a visual change in the infrared spectra. Firstly, phosphoric acid consumes OH from Al–OH bonds, and then the Al^{3+} is released from the kaolinite structure forming $AlPO_4$ in the solution. The bonds represented in the spectrum with aluminium contributions (Al–OH and Si–O–Al stretching) decrease even with poor attacks, and this effect becomes more pronounced with higher mineral acid concentration or elevated CA temperature. The Si–O–Al stretching vibrations (525 cm^{-1}) exhibit a slight shifting of their peaks from 525 cm^{-1} original kaolinite contribution to 528 cm^{-1} for KP_4_8_60, to 533 cm^{-1} for KP_12_8_90 and 535 cm^{-1} for

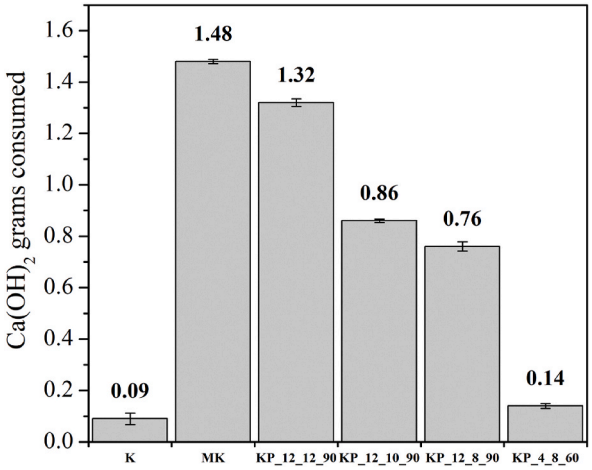

Fig. 8. Amount of consumed portlandite in the modified Chapelle test for K, MK, KP_12_12_90, KP_12_10_90, KP_12_8_90 and KP_4_8_60.

KP_12_12_90, as shown in Fig. 7e. This could be explained by the different chemical environment formed by the new neighbouring Si–O–Si units primarily shifted from Q^3 to Q^4 configurations, for the remaining Si–O–Al bonds.

3.2. Reactivity assessment

3.2.1. Modified Chapelle test

The fixed amount of $Ca(OH)_2$ obtained in the modified Chapelle test (Fig. 8) determined the pozzolanic activity of the dealuminated and amorphised kaolinite samples. The pozzolanity acquirement is based on generating reactive Si and Al units from pozzolan materials, which subsequently react with $Ca(OH)_2$ producing calcium silicate and aluminate hydrated phases [69]. In this case, MK and KP_12_12_90 are the samples with a major capacity of consuming $Ca(OH)_2$, falling within the range of 1.5 and 1.3 g of $Ca(OH)_2$ consumed, respectively, a value that comprises excellent pozzolanic material [70]. As other authors confirmed, MK consumes between 1 and 1.7 g of portlandite in Chapelle tests [30,60]. The variation reported in the literature is attributed to the diverse treatment temperatures and the original composition of the kaolin used in the experiments (kaolinite percentage). KP_12_12_90 performed in the same range of Ca consumption, suggesting a very reactive material. To consider an SCM as a pozzolanic material, it must have consumed 660 mg of $Ca(OH)_2$ during modified Chapelle test [30]. Consequently, KP_12_10_90 and KP_12_8_90 can also be distinguished as pozzolanic material since they consumed 0.86 g and 0.76 g of $Ca(OH)_2$, respectively. Their reactivity performances are much lower than KP_12_12_90 and calcined clays. Nonetheless, raw kaolin consumed only 0.09 g of $Ca(OH)_2$ and KP_4_8_60 consumed 0.14 g, hence their reactivity performances are almost the same. This is because they both share a very similar structure since the chemical activation for KP_4_8_60 results insufficient to alter the kaolinite content minimally.

3.2.2. R^3 test

Fig. 9 compiles the cumulative heat of the SCM-$Ca(OH)_2$ system measured in $J{\cdot}g^{-1}$ of SCM from the R^3 test. K and KP_4_8_60 samples are considered inert under R^3 test conditions since they show a very low amount of accumulated heat for 144 h (Heat flow, $W{\cdot}g^{-1}$, can be seen in Fig. A1 also). Nonetheless, KP_4_8_60 does not reach a plateau as it is an SCM with very poor reactivity with an exothermic heat value of around 67 J g^{-1}, suggesting an unfinished reaction. Some authors have performed earlier R^3-modified tests at 50 °C since it can increase the SCM reactivity effectiveness, enhancing knowledge of low-reactivity materials [71]. The calorimetric curves of KP_12_12_90, KP_12_10_90 and KP_12_8_90 samples exhibit an increasing trend over time. This is attributed to the fact that these samples contain progressively higher amounts of available SCM, which is capable of undergoing reactions with Ca(OH)2, resulting in the observed rise in cumulative heat output. At 144 h, KP_12_12_90 SCM reaches 522 J g^{-1}, KP_12_10_90 reaches 224 J g^{-1}, KP_12_8_90 reaches 178 J g^{-1} and MK reaches 963 J·g-1. KP_12_10_90 and KP_12_8_90 result in a partially reactive material, while KP_12_12_90 reaches promising reactivity values and MK reaffirmed to perform as further reactive kaolin. This corroborates the modified Chapelle test results as well as the amorphization data recorded in the structural characterisation. However, the KP_12_12_90 modified Chapelle results of portlandite consumption reveal the SCM to perform almost as MK in reactivity terms, but in comparison with the cumulative heat recorded in the TAM Air experiment, a great difference can be appreciated. The overestimation is probably associated with an acceleration of the pozzolanic reaction kinetics (the modified Chapelle test performed at 90 °C and isothermal calorimetry at 40 °C) and thereby of the $Ca(OH)_2$ consumption [60].

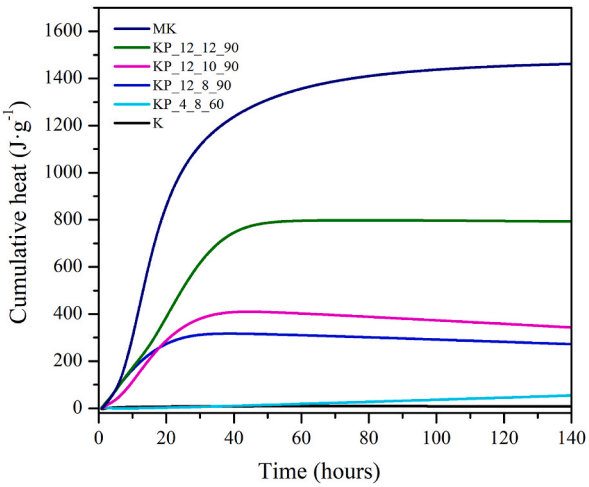

Fig. 9. The cumulative heat release of the SCM pozzolanic reaction of K, MK, KP_12_12_90, KP_12_10_90, and KP_12_8_90 samples.

Table 3
Ranges/values of cumulative heat release for common SCMs and chemically activated kaolinites.

SCM	Cumulative heat release range/value (J·g^{-1} SCM)	References
Calcined clays	450–900	[34,35,72–75]
Furnace slag	350–500	[34,35,72–75]
Silica fume	350–600	[34,35,72–74]
Fly ash	200–350	[34,35,72–75]
Limestone	0	[34,74]
Quartz	20–60	[34,74,75]
Ground lightweight aggregates	215–300	[34]
Volcanic ashes	236–311	[72]
Basalt fines	19	[34]
Ground bottom ashes	150–250	[72]
KP_12_12_90	522	–
KP_12_10_90	224	–
KP_12_8_90	178	–
KP_4_8_60	67	–

The 7-day R^3 results that exceed the limit of 160 J g^{-1} of SCM are classified as a pozzolanic-reactive material with a 90% confidence level, according to RILEM TC 267 [72]. Considering the same cumulative heat at 6 days as at 7 days, all the chemically activated kaolin submitted at 12 h of reaction time at 90 °C, can be classified as a reactive SCM, as well as MK. For a better understanding of the reactive capability of the chemically activated kaolins, Table 3 offers a classification of them among already-known SCMs tested with the R^3 test by different authors. In addition to the current study, P. Suraneni classified the SCM reactivities depending on the cumulative heat ranges: <120 J g^{-1} SCM – inert; 120 J g^{-1} SCM to 370 J g^{-1} SCM – less reactive; >370 J g^{-1} – more reactive [34]. This proposes KP_12_12_90 as a high pozzolanic reactive.

3.2.3. Specific surface area analysis

The BET method was employed to assess the specific surface area, a critical parameter for comprehending the reactivity performance of chemically activated kaolinites (Fig. 10). Eventually, the increase in the surface area involves an improvement in the material's reactivity. Focusing on the study case, a slight decrease on the specific surface area in the MK (8.97 m^2 g^{-1}) in comparison with K (9.98 m^2 g^{-1}) is observed. This diminishment is attributed to particle aggregation and sintering during calcination [76]. In accordance with the specific surface area values of the chemically activated kaolinites, the Al removal produces an extended increase of the reactive surface area, improving the reactivity behaviour as well. KP_4_8_60 shows a great improvement (~40%) on its specific surface area considering that it is the less intensive CA. KP_12_12_60 doubles the specific surface area in comparison with K. KP_12_10_90 and KP_12_12_90 reached 49.92 m^2 g^{-1} and 55.25 m^2 g^{-1}, respectively, interesting values which remarked again the temperature importance in CA procedures. Hence, the reactivity increase of chemically activated kaolinite could be explained by the amorphization produced by the dealumination, as well as the increase of the specific surface area acquirement.

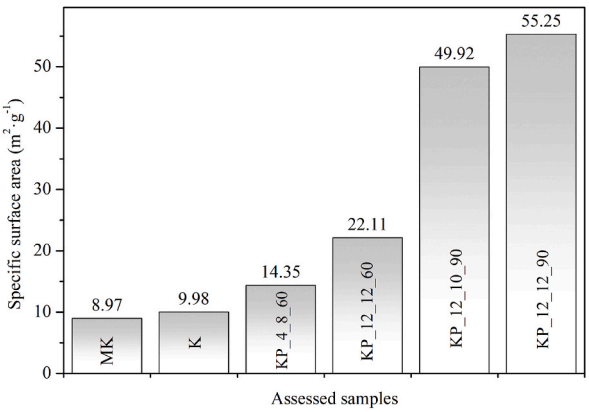

Fig. 10. The specific surface area values of MK, K, KP_4_8_60, KP_12_12_60, KP_12_10_90 and KP_12_12_90.

4. Conclusions

This work presents a novel way to convert kaolinite into an amorphous solid phase with the potential ability to perform suitably as a cement precursor. The kaolinite activation using phosphoric acid was achieved at different degrees through three main parameters (temperature, reaction time, and phosphoric acid concentration). Based on the experimental results obtained, the following conclusions can be drawn:

- The dealumination phenomenon was observed by every technique used, but it was accurately quantified by ICP-OES. This technique suggested that submitting kaolin into treatments at 60 °C or 90 °C can significantly increase the percentage of dissolved aluminium to 50%, meanwhile, the concentration causes variations around 5% only. The increase of K–H_3PO_4 reaction time augmented the dealumination linearly. The SiO_2 dissolved content was smaller than 0.5% after every chemical treatment. In the FTIR spectra, every peak comprised of Al contributions was severely diminished through intensive chemical attacks. In the TGA and MAS NMR studies, the diminishments of the Al contributions were also observed once dealumination took place.
- The evolution of the crystalline content into an amorphous phase was observed through 2 techniques: (i) X-ray diffraction showed a certain level of amorphization which increases as chemical activations were intensively augmented. (ii) ^{29}Si MAS NMR plotted the change from Q^3 to Q^4 in the Si environments of kaolinite. This was caused by the Al removal. Subsequently, Si–O–Si interlayered bonds were established randomly.
- In reactivity terms, the sample KP_12_12_90 achieved a similar range of cumulative heat than Silica fume, falling in the range nearby calcined clays, performing as a highly pozzolanic material according to R^3 test knowledge. The modified Chapelle test results were in accordance with R^3 suggesting KP_12_12_90 to be a good Portlandite consumer. KP_12_8/10_90 were considered as less reactive materials, and KP_4_8_60 was an inert clay. This implies an intensive chemical treatment to achieve a reactive precursor. Therefore, a good estimation of the reactivity of kaolinites can be made based on the modified Chapelle test in contrast with the R^3 test.

This paper provides optimised parameters for the obtention of a novel SCM or precursor based on submitting kaolinite clay to chemical treatments. The dealumination resulted to be the key for the kaolinitic structure amorphization and specific surface area enhancement, improving the reaction capability on the pertinent clay. The main drawback is the mass loss attributed to the dissolution of alumina, which is required to produce the activation. Nonetheless, the reactivity performances of the most intensively treated sample showed interesting values.

Funding

This work is partially supported by the Spanish Government with the Grants PID2021-125810OB-C21 and TED2021-129718B–I00 funded by MCIN/AEI/10.13039/501100011033, by "ERDF A way of making Europe", and by the "European Union NextGenerationEU/PRTR" and the Catalan Government with the Grant 2021 SGR 00708. Furthermore, the Agència de Gestió d'Ajuts Universitaris i de Recerca (AGAUR) contributed through Mr Jofre Mañosa's PhD grant (FI 2020).

CRediT authorship contribution statement

Adrian Alvarez-Coscojuela: Writing – review & editing, Writing – original draft, Visualization, Investigation, Formal analysis, Data curation. **Jofre Mañosa:** Writing – review & editing, Visualization, Resources, Data curation. **Joan Formosa:** Writing – review & editing, Visualization, Supervision, Funding acquisition. **Josep Maria Chimenos:** Writing – review & editing, Visualization, Supervision, Resources, Funding acquisition, Conceptualization.

Declaration of competing interest

The authors declare that they have no known competing financial interests or personal relationships that could have appeared to influence the work reported in this paper.

Data availability

Data will be made available on request.

Acknowledgements

The authors would like to thank the Catalan Government for the quality accreditation given to their research group DIOPMA (2021 SGR 00708). DIOPMA is a certified agent TECNIO in the category of technology developers from the Government of Catalonia. The authors are grateful to the companies Minerals i Derivats, S.A. and COM-CAL for the supply of the raw kaolin as well as CCiTUB and SCAI for the equipment or measurements of XRD, ICP-OES, BET and MAS NMR. Mr Jofre Mañosa is grateful to the Catalan Government for his research Grant, FI-DGR 2020. The authors acknowledge the support of CYTED Network ECoEICo—Circular Economy as a Strategy for a More Sustainable Construction Industry and the COST Action CircularB—Implementation of Circular Economy in the Built Environment.

Appendix A. Supplementary data

Supplementary data to this article can be found online at https://doi.org/10.1016/j.jobe.2024.109051.

References

[1] D.N. Huntzinger, T.D. Eatmon, A life-cycle assessment of Portland cement manufacturing: comparing the traditional process with alternative technologies,, J. Clean. Prod. 17 (2009) 668–675, https://doi.org/10.1016/j.jclepro.2008.04.007.

[2] L.K. Turner, F.G. Collins, Carbon dioxide equivalent (CO_2-e) emissions: a comparison between geopolymer and OPC cement concrete,, Construct. Build. Mater. 43 (2013) 125–130, https://doi.org/10.1016/j.conbuildmat.2013.01.023.

[3] R. Snellings, G. Mertens, J. Elsen, Supplementary cementitious materials, Rev. Mineral. Geochem. 74 (2012) 211–278, https://doi.org/10.2138/rmg.2012.74.6.

[4] B. Lothenbach, K. Scrivener, R.D. Hooton, Supplementary cementitious materials, Cement Concr. Res. 41 (2011) 1244–1256, https://doi.org/10.1016/j.cemconres.2010.12.001.

[5] A. Arrigoni, D.K. Panesar, M. Duhamel, T. Opher, S. Saxe, I.D. Posen, H.L. MacLean, Life cycle greenhouse gas emissions of concrete containing supplementary cementitious materials: cut-off vs. substitution, J. Clean. Prod. 263 (2020), https://doi.org/10.1016/j.jclepro.2020.121465.

[6] J. Duchesne, Alternative supplementary cementitious materials for sustainable concrete structures: a review on characterization and properties, Waste Biomass Valorization 12 (2021) 1219–1236, https://doi.org/10.1007/s12649-020-01068-4.

[7] J.L. Provis, Alkali-activated materials, Cement Concr. Res. 114 (2018) 40–48, https://doi.org/10.1016/j.cemconres.2017.02.009.

[8] B. Ayati, D. Newport, H. Wong, C. Cheeseman, Acid activated smectite clay as pozzolanic supplementary cementitious material, Cem Concr Res, 162 106969 (2022), https://doi.org/10.1016/j.cemconres.2022.106969.

[9] S. Guggenheim, R.T. Martin, Report Definition Of Clay And Clay Mineral: Joint Report Of The Aipea Nomenclature And Cms Nomenclature CommitteeS, 1995.

[10] A. Ito, R. Wagai, Global distribution of clay-size minerals on land surface for biogeochemical and climatological studies, Sci. Data 4 (2017), https://doi.org/10.1038/sdata.2017.103.

[11] L.N. Tchadjie, S.O. Ekolu, Enhancing the reactivity of aluminosilicate materials toward geopolymer synthesis, J. Mater. Sci. 53 (2018) 4709–4733, https://doi.org/10.1007/s10853-017-1907-7.

[12] M.F. Brigatti, E. Galán, B.K.G. Theng, Structure and mineralogy of clay minerals. https://doi.org/10.1016/B978-0-08-098258-8.00002-X, 2013.

[13] J. Mañosa, J.C. la Rosa, A. Silvello, A. Maldonado-Alameda, J.M. Chimenos, Kaolinite structural modifications induced by mechanical activation, Appl Clay Sci, 238 106918 (2023), https://doi.org/10.1016/j.clay.2023.106918.

[14] A. Tironi, M.A. Trezza, A.N. Scian, E.F. Irassar, Assessment of pozzolanic activity of different calcined clays, Cem. Concr. Compos. 37 (2013) 319–327, https://doi.org/10.1016/j.cemconcomp.2013.01.002.

[15] F. Moodi, A.A. Ramezanianpour, A.S. Safavizadeh, Evaluation of the optimal process of thermal activation of kaolins, Sci. Iran. 18 (2011) 906–912, https://doi.org/10.1016/j.scient.2011.07.011.

[16] I. Tole, K. Habermehl-Cwirzen, A. Cwirzen, Mechanochemical activation of natural clay minerals: an alternative to produce sustainable cementitious binders – review, Mineral. Petrol. 113 (2019) 449–462, https://doi.org/10.1007/s00710-019-00666-y.

[17] J. Mañosa, A. Alvarez-Coscojuela, J. Marco-Gibert, A. Maldonado-Alameda, J.M. Chimenos, Enhancing reactivity in muscovitic clays: mechanical activation as a sustainable alternative to thermal activation for cement production, Appl Clay Sci, 250 107266 (2024), https://doi.org/10.1016/j.clay.2024.107266.

[18] J. Macfarlane, A Review On Use Of Metakaolin In Concrete, 2013.

[19] M.C.G. Juenger, R. Snellings, S.A. Bernal, Supplementary cementitious materials: new sources, characterization, and performance insights, Cement Concr. Res. 122 (2019) 257–273, https://doi.org/10.1016/j.cemconres.2019.05.008.

[20] I. Tole, K. Habermehl-Cwirzen, M. Rajczakowska, A. Cwirzen, Activation of a raw clay by mechanochemical process-effects of various parameters on the process efficiency and cementitious properties, Materials 11 (2018), https://doi.org/10.3390/ma11101860.

[21] A. Souri, H. Kazemi-Kamyab, R. Snellings, R. Naghizadeh, F. Golestani-Fard, K. Scrivener, Pozzolanic activity of mechanochemically and thermally activated kaolins in cement, Cement Concr. Res. 77 (2015) 47–59, https://doi.org/10.1016/j.cemconres.2015.04.017.

[22] J. Mañosa, A.M. Gómez-Carrera, A. Svobodova-Sedlackova, A. Maldonado-Alameda, A. Fernández-Jiménez, J.M. Chimenos, Potential reactivity assessment of mechanically activated kaolin as alternative cement precursor, Appl. Clay Sci. 228 (2022), https://doi.org/10.1016/j.clay.2022.106648.

[23] S. Louati, W. Hajjaji, S. Baklouti, B. Samet, Structure and properties of new eco-material obtained by phosphoric acid attack of natural Tunisian clay, Appl. Clay Sci. 101 (2014) 60–67, https://doi.org/10.1016/j.clay.2014.07.015.

[24] H. Lin, H. Liu, Y. Li, X. Kong, Properties and reaction mechanism of phosphoric acid activated metakaolin geopolymer at varied curing temperatures, Cement Concr. Res. 144 (2021), https://doi.org/10.1016/j.cemconres.2021.106425.

[25] Y.S. Wang, J.G. Dai, Z. Ding, W.T. Xu, Phosphate-based geopolymer: formation mechanism and thermal stability, Mater. Lett. 190 (2017) 209–212, https://doi.org/10.1016/j.matlet.2017.01.022.

[26] V. Mathivet, J. Jouin, A. Gharzouni, I. Sobrados, H. Celerier, S. Rossignol, M. Parlier, Acid-based geopolymers: understanding of the structural evolutions during consolidation and after thermal treatments, J. Non-Cryst. Solids 512 (2019) 90–97, https://doi.org/10.1016/j.jnoncrysol.2019.02.025.

[27] X. Li, R. Snellings, M. Antoni, N.M. Alderete, M. Ben Haha, S. Bishnoi, Ö. Cizer, M. Cyr, K. De Weerdt, Y. Dhandapani, J. Duchesne, J. Haufe, D. Hooton, M. Juenger, S. Kamali-Bernard, S. Kramar, M. Marroccoli, A.M. Joseph, A. Parashar, C. Patapy, J.L. Provis, S. Sabio, M. Santhanam, L. Steger, T. Sui, A. Telesca, A. Vollpracht, F. Vargas, B. Walkley, F. Winnefeld, G. Ye, M. Zajac, S. Zhang, K.L. Scrivener, Reactivity tests for supplementary cementitious materials: RILEM TC 267-TRM phase 1, Materials and Structures/Materiaux et Constructions 51 (2018), https://doi.org/10.1617/s11527-018-1269-x.

[28] E. Ferraz, S. Andrejkovičová, W. Hajjaji, A.L. Velosa, A.S. Silva, F. Rocha, Pozzolanic activity of metakaolins by the French standard of the modified Chapelle test: a direct methodology,, Acta Geodyn. Geomater. 12 (2015) 289–298, https://doi.org/10.13168/AGG.2015.0026.

[29] A. Ababneh, F. Matalkah, B. Matalkeh, Effects of kaolin characteristics on the mechanical properties of alkali-activated binders, Construct. Build. Mater. 318 (2022), https://doi.org/10.1016/j.conbuildmat.2021.126020.

[30] J. Pontes, A. Santos Silva, P. Faria, Evaluation of pozzolanic reactivity of artificial pozzolans, Materials Science Forum, Trans Tech Publications Ltd (2013) 433–438. https://doi.org/10.4028/www.scientific.net/MSF.730-732.433.

[31] F. Avet, R. Snellings, A. Alujas Diaz, M. Ben Haha, K. Scrivener, Development of a new rapid, relevant and reliable (R^3) test method to evaluate the pozzolanic reactivity of calcined kaolinitic clays, Cement Concr. Res. 85 (2016) 1–11, https://doi.org/10.1016/j.cemconres.2016.02.015.

[32] M. Maier, N. Beuntner, K.C. Thienel, Mineralogical characterization and reactivity test of common clays suitable as supplementary cementitious material, Appl Clay Sci, 202 105990 (2021), https://doi.org/10.1016/j.clay.2021.105990.

[33] American Society for Testing and Materials, Astm C1897–20: standard test methods for measuring the reactivity of supplementary cementitious materials by isothermal calorimetry and bound water measurements. https://doi.org/10.1520/C1897-20, 2020.

[34] P. Suraneni, A. Hajibabaee, S. Ramanathan, Y. Wang, J. Weiss, New insights from reactivity testing of supplementary cementitious materials, Cem. Concr. Compos. 103 (2019) 331–338, https://doi.org/10.1016/j.cemconcomp.2019.05.017.

[35] S. Ramanathan, H. Moon, M. Croly, C.W. Chung, P. Suraneni, Predicting the degree of reaction of supplementary cementitious materials in cementitious pastes using a pozzolanic test, Construct. Build. Mater. 204 (2019) 621–630, https://doi.org/10.1016/j.conbuildmat.2019.01.173.

[36] F.K. Crundwell, On the mechanism of the dissolution of quartz and silica in aqueous solutions, ACS Omega 2 (2017) 1116–1127, https://doi.org/10.1021/acsomega.7b00019.

[37] V. Dimitrov, T. Komatsu, Classification of simple oxides: a polarizability approach,, J. Solid State Chem. 163 (2002) 100–112, https://doi.org/10.1006/jssc.2001.9378.

[38] O. Allahdin, M. Wartel, G. Tricot, B. Revel, A. Boughriet, Hydroxylation and dealumination of a metakaolinite-rich brick under acid conditions, and their influences on metal adsorption: one- and two-dimensional (^{1}H, ^{27}Al, ^{23}Na, ^{29}Si) MAS NMR, and FTIR studies, Microporous Mesoporous Mater. 226 (2016) 360–368, https://doi.org/10.1016/j.micromeso.2016.02.028.

[39] Y. Zhou, H. Cheng, C. Wei, Y. Zhang, Effect of acid activation on structural evolution and surface charge of different derived kaolinites, Appl. Clay Sci. 203 (2021), https://doi.org/10.1016/j.clay.2021.105997.

[40] M. Zribi, B. Samet, S. Baklouti, Investigation of dealumination in phosphate-based geopolymer formation process: factor screening and optimization, Minerals 12 (2022), https://doi.org/10.3390/min12091104.

[41] M. Khabbouchi, K. Hosni, E. Srasra, Physico-chemical characterization of modified Tunisian kaolin by phosphoric acid, Surf. Eng. Appl. Electrochem. 54 (2018) 219–226, https://doi.org/10.3103/S1068375518020072.

[42] R. Fernandez, F. Martirena, K.L. Scrivener, The origin of the pozzolanic activity of calcined clay minerals: a comparison between kaolinite, illite and montmorillonite,, Cement Concr. Res. 41 (2011) 113–122, https://doi.org/10.1016/j.cemconres.2010.09.013.

[43] B. Zhang, H. Guo, L. Deng, W. Fan, T. Yu, Q. Wang, Undehydrated kaolinite as materials for the preparation of geopolymer through phosphoric acid-activation, Appl Clay Sci, 199 105887 (2020), https://doi.org/10.1016/j.clay.2020.105887.

[44] T.P.M. Goumans, A. Wander, W.A. Brown, C.R.A. Catlow, Structure and stability of the (001) α-quartz surface, Phys. Chem. Chem. Phys. 9 (2007) 2146–2152, https://doi.org/10.1039/b701176h.

[45] H. Hartati, A. Purwaningsih, T.S. Tjahjandarie, N.H. Saputri, I.S. Puspitasari, C.N. Lamanele, A.A. Sa'adah, A.S. Haque, D.Z. Mardho, Synthesis of amorphous aluminosilicate from impure Indonesian kaolin, Open Chem. 18 (2020) 295–302, https://doi.org/10.1515/chem-2020-0033.

[46] P. Zemenová, A. Kloužková, M. Kohoutková, R. Král, Investigation of the first and second dehydroxylation of kaolinite. J Therm Anal Calorim, Kluwer Academic Publishers, 2014, pp. 633–639, https://doi.org/10.1007/s10973-014-3748-9.

[47] C.J. Johnston, R.A. Pepper, W.N. Martens, S. Couperthwaite, Relationship between thermal dehydroxylation and aluminium extraction from a low-grade kaolinite: role of clay chemistry and crystallinity, Hydrometallurgy 214 (2022), https://doi.org/10.1016/j.hydromet.2022.105967.

[48] A. Shvarzman, K. Kovler, G.S. Grader, G.E. Shter, The effect of dehydroxylation/amorphization degree on pozzolanic activity of kaolinite,, Cement Concr. Res. 33 (2003) 405–416, https://doi.org/10.1016/S0008-8846(02)00975-4.

[49] P. Alfonso, L.A. Penedo, M. García-Valles, S. Martínez, A. Martínez, J.E. Trujillo, Thermal behaviour of kaolinitic raw materials from San José (Oruro, Bolivia), J. Therm. Anal. Calorim. 147 (2022) 5413–5421, https://doi.org/10.1007/s10973-022-11245-3.

[50] F. Lagno, G.P. Demopoulos, The stability of hydrated aluminium phosphate, $AlPO_4{\cdot}1.5H_2O$,, Environ. Technol. 27 (2006) 1217–1224, https://doi.org/10.1080/09593332708618735.

[51] E. AdabiFiroozjaei, P. Koshy, C.C. Sorrell, Effects of $AlPO_4$ addition on the corrosion resistance of andalusite-based low-cement castables with molten Al-alloy, J. Eur. Ceram. Soc. 33 (2013) 1067–1075, https://doi.org/10.1016/j.jeurceramsoc.2012.11.005.

[52] B. Walkley, J.L. Provis, Solid-state nuclear magnetic resonance spectroscopy of cements, Mater Today Adv 1 (2019) 100007, https://doi.org/10.1016/j.mtadv.2019.100007.

[53] A. Escudero Belmonte, RMN aplicada al estado sólido, Anales de La Real Sociedad Española de Química, 2004, pp. 27–36.

[54] H.P. He, J.. G. Guo, J.. X. Zhu, C. Hu, ^{29} Si and ^{27} Al MAS NMR study of the thermal transformations of kaolinite from North China, Clay Miner. 38 (2003) 551–559, https://doi.org/10.1180/0009855033840114.

[55] H. Celerier, J. Jouin, A. Gharzouni, V. Mathivet, I. Sobrados, N. Tessier-Doyen, S. Rossignol, Relation between working properties and structural properties from ^{27} Al, ^{29} Si and ^{31} P NMR and XRD of acid-based geopolymers from 25 to 1000°C, Mater. Chem. Phys. 228 (2019) 293–302, https://doi.org/10.1016/j.matchemphys.2019.02.049.

[56] W. Loewenstein, The distribution of aluminum in the tetrahedra of silicates and aluminates.,, Am. Mineral. 39 (1954) 92–96.

[57] B. Walkley, Geopolymers, Encyclopedia of Earth Sciences Series 37 (2020) 1633–1656, https://doi.org/10.1007/978-3-319-12127-7_299-1.

[58] F. Souayfan, E. Rozière, M. Paris, D. Deneele, A. Loukili, C. Justino, ^{29}Si and ^{27}Al MAS NMR spectroscopic studies of activated metakaolin-slag mixtures, Construct. Build. Mater. 322 (2022), https://doi.org/10.1016/j.conbuildmat.2022.126415.

[59] A.Á.B. Maia, R.S. Angélica, R. de Freitas Neves, H. Pöllmann, C. Straub, K. Saalwächter, Use of ^{29}Si and ^{27}Al MAS NMR to study thermal activation of kaolinites from Brazilian Amazon kaolin wastes, Appl. Clay Sci. 87 (2014) 189–196, https://doi.org/10.1016/j.clay.2013.10.028.

[60] S. Hollanders, R. Adriaens, J. Skibsted, Ö. Cizer, J. Elsen, Pozzolanic reactivity of pure calcined clays, Appl Clay Sci 132–133 (2016) 552–560, https://doi.org/10.1016/j.clay.2016.08.003.

[61] P. Ptáček, F. Frajkorová, F. Šoukal, T. Opravil, Kinetics and mechanism of three stages of thermal transformation of kaolinite to metakaolinite, Powder Technol. 264 (2014) 439–445, https://doi.org/10.1016/j.powtec.2014.05.047.

[62] A. Tironi, M.A. Trezza, E.F. Irassar, A.N. Scian, Thermal treatment of kaolin: effect on the pozzolanic activity, Procedia Materials Science 1 (2012) 343–350, https://doi.org/10.1016/j.mspro.2012.06.046.

[63] B.J. Saikia, G. Parthasarathy, Fourier transform infrared spectroscopic characterization of kaolinite from Assam and Meghalaya, northeastern India, J. Mod. Phys. 1 (2010) 206–210, https://doi.org/10.4236/jmp.2010.14031.

[64] M.A. Legodi, D. de Waal, Raman spectroscopic study of ancient South African domestic clay pottery, Spectrochim. Acta Mol. Biomol. Spectrosc. 66 (2007) 135–142, https://doi.org/10.1016/j.saa.2006.02.059.

[65] C.M. Müller, B. Pejcic, L. Esteban, C.D. Piane, M. Raven, B. Mizaikoff, Infrared attenuated total reflectance spectroscopy: an innovative strategy for analyzing mineral components in energy relevant systems, Sci. Rep. 4 (2014) 1–11, https://doi.org/10.1038/srep06764.

[66] W.K.W. Lee, J.S.J. Van Deventer, Use of infrared spectroscopy to study geopolymerization of heterogeneous amorphous aluminosilicates, Langmuir 19 (2003) 8726–8734, https://doi.org/10.1021/la026127e.

[67] M. Hoch, A. Bandara, Determination of the adsorption process of tributyltin (TBT) and monobutyltin (MBT) onto kaolinite surface using Fourier transform infrared (FTIR) spectroscopy, Colloids Surf. A Physicochem. Eng. Asp. 253 (2005) 117–124, https://doi.org/10.1016/j.colsurfa.2004.10.118.

[68] C. Bich, J. Ambroise, J. Péra, Influence of degree of dehydroxylation on the pozzolanic activity of metakaolin, Appl. Clay Sci. 44 (2009) 194–200, https://doi.org/10.1016/j.clay.2009.01.014.

[69] T. Seiffarth, M. Hohmann, K. Posern, C. Kaps, Effect of thermal pre-treatment conditions of common clays on the performance of clay-based geopolymeric binders, Appl. Clay Sci. 73 (2013) 35–41, https://doi.org/10.1016/j.clay.2012.09.010.

[70] A. Kamalakar Mali, P. Nanthagopalan, Development of a framework for the selection of best sugarcane bagasse ash from different sources for use in the cement-based system: a rapid and reliable path, Constr Build Mater, 293 123386 (2021), https://doi.org/10.1016/j.conbuildmat.2021.123386.

[71] S. Ramanathan, L.R. Pestana, P. Suraneni, Reaction kinetics of supplementary cementitious materials in reactivity tests, Cemento 8 (2022) 100022, https://doi.org/10.1016/j.cement.2022.100022.

[72] J. Yoon, K. Jafari, R. Tokpatayeva, S. Peethamparan, J. Olek, F. Rajabipour, Characterization and quantification of the pozzolanic reactivity of natural and non-conventional pozzolans, Cem Concr Compos, 133 104708 (2022), https://doi.org/10.1016/j.cemconcomp.2022.104708.

[73] D. Londono-Zuluaga, A. Gholizadeh-Vayghan, F. Winnefeld, F. Avet, M. Ben Haha, S.A. Bernal, Ö. Cizer, M. Cyr, S. Dolenec, P. Durdzinski, J. Haufe, D. Hooton, S. Kamali-Bernard, X. Li, A.T.M. Marsh, M. Marroccoli, M. Mrak, Y. Muy, C. Patapy, M. Pedersen, S. Sabio, S. Schulze, R. Snellings, A. Telesca, A. Vollpracht,

G. Ye, S. Zhang, K.L. Scrivener, Report of RILEM TC 267-TRM phase 3: validation of the R^3 reactivity test across a wide range of materials, Materials and Structures/Materiaux et Constructions 55 (2022), https://doi.org/10.1617/s11527-022-01947-3.

[74] P. Suraneni, J. Weiss, Examining the pozzolanicity of supplementary cementitious materials using isothermal calorimetry and thermogravimetric analysis, Cem. Concr. Compos. 83 (2017) 273–278, https://doi.org/10.1016/j.cemconcomp.2017.07.009.

[75] S. Al-Shmaisani, R.D. Kalina, R.D. Ferron, M.C.G. Juenger, Critical assessment of rapid methods to qualify supplementary cementitious materials for use in concrete, Cement Concr. Res. 153 (2022) 106709, https://doi.org/10.1016/j.cemconres.2021.106709.

[76] B. Ilić, V. Radonjanin, M. Malešev, M. Zdujić, A. Mitrović, Effects of mechanical and thermal activation on pozzolanic activity of kaolin containing mica, Appl. Clay Sci. 123 (2016) 173–181, https://doi.org/10.1016/j.clay.2016.01.029.